Journal of Coastal Research	6	4	961-980	Fort Lauderdale, Florida	Fall 1990

Resuspension of Estuarial Fine Sediments by Tethered Wings

Scott A. Jenkins and Joseph Wasyl

Scripps Institution of
Oceanography, A-009
La Jolla, CA 92093, USA

ABSTRACT

JENKINS, S.A. and WASYL, J., 1990. Resuspension of estuarial fine sediments by tethered wings. *Journal of Coastal Research*, 6(4), 961-980. Fort Lauderdale (Florida). ISSN 0749-0208.

A theory and companion experiment are given which describe the resuspension of fine sediments by the action of wings moored near the bottom of an estuary. Calculations by matched inner and outer image expansions indicate that the vortex system of a wing can exert two distinct effects on estuarial sedimentation: (1) it can elevate the shear stresses in the neighborhood of the wing by a sufficient amount to induce erosion of partially consolidated layers of the bottom; and, (2) it can promote vertical transport to either enhance or inhibit downstream deposition. Deposition in the wake trail is found to be dependent upon the direction of the lift force generated by the wing. Wings which produce a downward lift force deplete the region adjacent to the bottom of suspended sediment and thereby diminish downstream deposition. Conversely, wings generating an upward lift force increase the density of suspended sediment near the bottom, thus increasing the rate of downstream deposition. Optimal wing configurations are formulated which maximize erosion and minimize deposition. Density measurements behind prototype wings are consistent with these theoretical expectations. Short term changes in bottom contours are in general agreement with predicted erosion in the inner domain, and with diminished accretion in the outer domain.

ADDITIONAL INDEX WORDS: *Cohesive sediment, silt, clay, flocculation, erosion, deposition, consolidation, accretion, fluid mud, entrainment, lutocline, Bingham fluid, diffusivity, scour, lifting line, image method, circulation, horseshoe-vortices.*

INTRODUCTION

The phenomenon of current scour due to vortical wakes shed from the support piles of bridges and other waterfront structures is well known, (COLLINS, 1980, and CHIEW and MELVILLE, 1987). Transport of suspended particles by near-wake vortices behind bluff bodies has been found to be especially vigorous in air, (MacLENNAN and VINCENT, 1982). Vortices from boat traffic have been observed to scour and resuspend fine sediments, (GARRAD and HEY, 1987). The work herein begins with the hypothesis that the vortex system of a moored wing might perturb sediment transport and cause similar scour features in the muddy bottom under steady or slowly varying estuarine flow. If wing induced scour is found to be sufficiently vigorous, it could emerge as a new concept among the paucity of passive technologies to maintain dredged harbors and waterways. Presently, active technologies amass a $2 billion worldwide annual maintenance dredging bill, (MARINE BOARD, 1983). Those costs are largely driven by dredge spoils disposal problems which would otherwise not exist with passive methods.

The wing vortex system appears to be especially well suited to influence sediment transport because it imparts a net vertical advection to the flow in reaction to the lift force, (LANCHESTER, 1908, PRANDTL and BETZ, 1927, and PRANDTL, 1931). This vertical advection (induced velocity) might be employed to either reduce or increase the net settling rates of silts and clays, depending upon the direction of the lift force, (JENKINS and SPARKS, 1985, and JENKINS, 1987). Because the preponderance of transport of these fine-grained sediments occurs near the bottom, (EINSTEIN and KRONE, 1961, and MEHTA, *et al.*, 1989), we are particularly interested in the case of a wing

in proximity to the immobile bed, *i.e.*, in ground effect, (LAGALLY, 1929, PRESMAK, 1977, and McCORMICK, 1979). Ground effect is generally considered to be the condition in which the wing is within one semi-span length of a solid plane boundary.

We seek analytic solutions to the wing induced perturbations on sediment transport and the bed response so that cause and effect relations might be readily established. Therefore it shall be necessary to make a number of idealizations with respect to both the sediment transport physics as well as the flow field produced by the wing. We employ a Fickian-based advection-diffusion transport model to provide a deterministic approach with sufficient kinematic detail to allow analytic progress on the problem at hand. These are the most widely adopted fine-sediment transport models in the published literature and have been validated by both laboratory data, (APMAN and RUMER, 1970), and field data, (KERSSENS *et al.*, 1979). They have been employed to account for transport over eroding or accreting beds, (LAMBERMONT and LEBON, 1978, and CHENG, 1985), and for the vertical and streamwise variability in transport, (MEI, 1969). The latter was constrained by the assumption that the settling velocity of the sediment, ω_o, is of the same order as the mean flow velocity, u_o. This rather unrealistic assumption for the case of fine-sediment transport has been circumvented herein by coordinate stretching based on the strength of the wing perturbation.

With regard to specifying the flow field around a wing moored near an estuarine bottom, there are two major difficulties: (1) viscosity; and (2) density stratification due to the abundance of suspended sediment near the bottom. Unfortunately, the recent wing theories which explicitly account for the effects of either viscosity or density stratification are numerical, *e.g.*, MOORE (1974), MATTEI and SANTORO (1974), STAUFENBIEL and KLEINERDAM (1980), PULLIN and PHILLIPS (1981) or SAFFMAN (1972), HILL (1975) and GREEN (1985), respectively. Analytic solutions for the flow field induced by a wing of finite span present one of the most intractable problems in aerodynamic theory, (VAN DYKE, 1975). Therefore we shall neglect stratification and approximate the local flow field as an inviscid singular perturbation in the wing aspect ratio, A_w, after VAN DYKE (1964). This is based on the premise that the wing circulation is large compared to ambient levels and that the rotational and irrotational parts of the flow do not interact. Difficulties associated with the no-slip condition at the bottom do not explicitly arise herein because the sediment-transport equations developed in the following sections rely on inviscid wing-theory only to specify the vertical component of the flow field. Details of the trailing vortex roll-up in the near wake of the wing provided by the analytic results of BATCHELOR (1964), SQUIRE (1965), GOVINDARAJU and SAFFMAN (1972), SAFFMAN (1973) and PHILLIPS (1981) do not appear at the order of approximation taken in the formulation of the sediment-transport equations below.

Formulation

Consider a fluid of density, ρ_F, transporting a suspension of uniform particles, each with a settling velocity relative to the fluid, ω_o, and a solid density, $\rho_q = 2.65$ g/cm^3. The density of the fluid-sediment mixture, ρ_m, may be written:

$$\rho_m = \rho_q N + (1\text{-}N)\rho_F \qquad (1)$$

where N is the volume concentration equal to the volume of sediment per volume of the fluid-sediment mixture. The density of the sediment component of this mixture, ρ, is sometimes referred to as the excess or bulk density and is defined:

$$\rho = \rho_q N \qquad (2)$$

Assume a uniform channel flow with a characteristic velocity u_o which varies slowly at angular frequency Ω_o over a flat cohesive surface on the plane $z = 0$, see Figure 1. At or below $z = 0$, the fluid-sediment mixture exhibits a non-zero cohesive yield stress, τ_c, and behaves as a viscoplastic. Above $z = 0$, the cohesive yield stress vanishes and the fluid-sediment mixture behaves as a fluid, i.e., unable to support shear stress at equilibrium. The sediment component density at $z = 0$ where the mixture first begins to exhibit a cohesive yield stress is, $\rho = \rho_c$.

The upper regions of the fluid, $z \geq h$, are relatively deficient of suspended sediment and may be characterized by some small ambient value, $\rho = \rho_t$. Because of settling under the

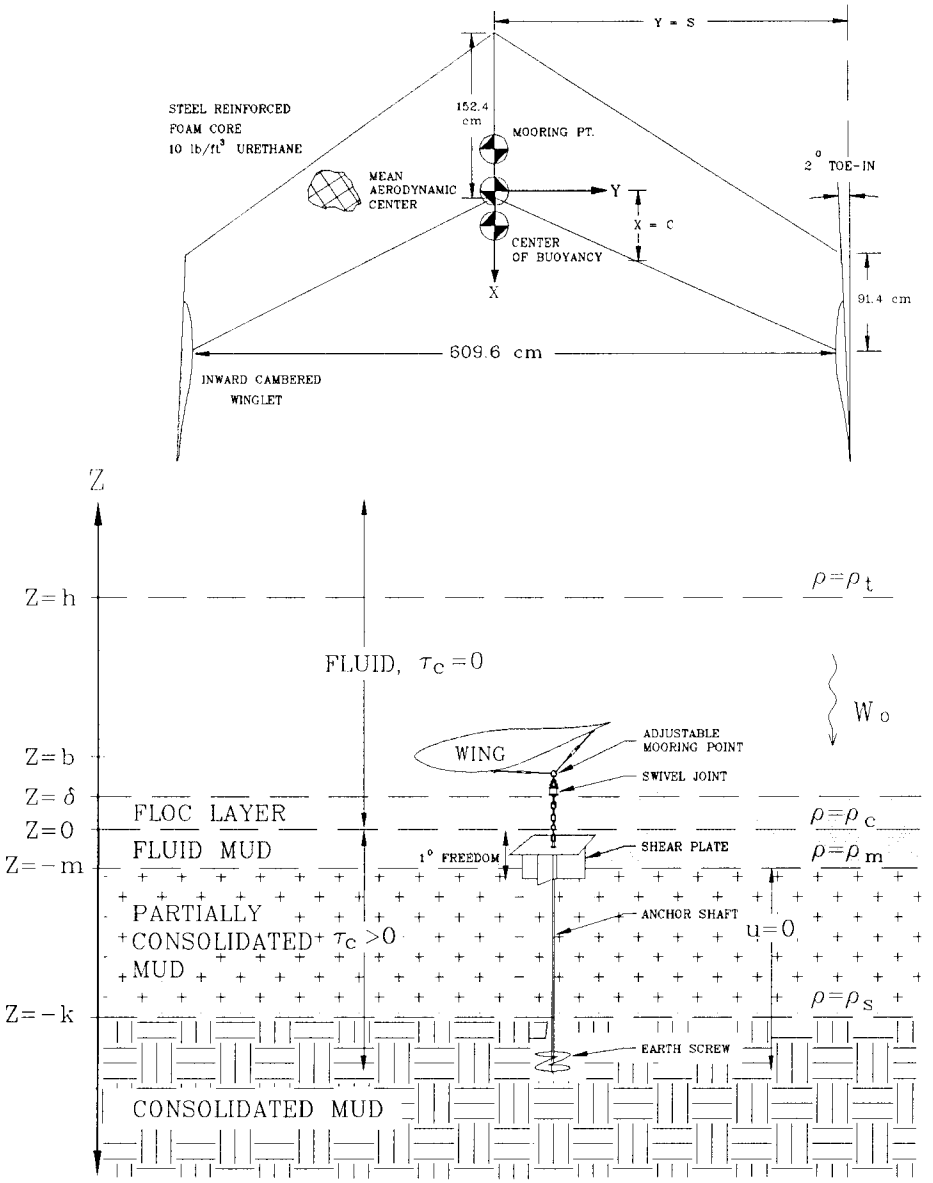

Figure 1. Conceptual diagram of the fluid bed interface with the wing and its mooring details.

influence of gravity, the abundance of suspended sediment begins to increase below z = δ, forming a non-cohesive floc layer as shown in Figure 1, (MEHTA and PARTHENIADES, 1975, and KRONE, 1978). The surface z = 0 may thus be considered a "lutocline", (DYER, 1985, and MEHTA, 1989).

Immediately below the lutocline, there is a rather thin layer of cohesive fluid mud between, $0 \leq z < -m$, which has a non-zero velocity, (KIRBY and PARKER, 1974, PARKER and KIRBY, 1982 and NICHOLS, 1985). Thus the lutocline at z = 0 between the fluid and the viscoplastic material is not a no-slip boundary. The dynamics of the fluid mud layer are still poorly understood when subjected to a moving

fluid. For analytic purposes, we shall assume that the lutocline at z = 0 is a stress free boundary much like a free surface, with the shear stresses resulting from the fluid motion appearing in the stress field of the fluid mud layer. This assumption relieves the wing induced velocity field on the fluid side of the lutocline interface from having to satisfy the no-slip condition at z = 0. The no-slip boundary thus appears at z = −m where the immobile, partially consolidated bottom begins.

Below the fluid mud layer, z < −m, the sediment is at rest and there is a progressive build up in sediment component density to some ultimate saturation value, $\rho = \rho_s$. This is due to consolidation and compaction under the weight of the overburden which proceeds at a rate characterized by $\rho_c K_s g$, where g is the acceleration of gravity and K_s is the sedimentation coefficient in seconds, (FUJITA, 1962). The portion of the cohesive bottom below the fluid mud layer for which $\rho_c \leq \rho < \rho_s$ shall be referred to as partially consolidated mud, while the fully consolidated mud in Figure 1 represents the oldest deposition which has reached final saturation density $\rho = \rho_s$.

Now superimpose a wing on the river flow at a distance z = b above the lutocline. Take the wing semi-span to be S. Assume the wing to be in ground effect so that b < S. Let the mean semi-cord be c so that the wing aspect ratio is $A_w = S/c$. We shall prescribe the sediment transport and the wing induced velocity field in an Eulerian frame with respect to Cartesian coordinates (x,y,z). The origin of this system is located at the intersection between the lutocline plane and a vertical projection from the mean aerodynamic center of the wing, see Figure 1. The axis o-z shall be positive vertically upward; the axis o-x is positive in the direction of the river channel flow; while the axis o-y is transverse to the mean channel flow in a right hand system.

With the problem posed in this way, the only horizontal variability will be that imposed by the wing over length scales the size of a wing semi-span. On the other hand, the density field is structured vertically, with strong variability near the lutocline over length scales of the order of the floc layer thickness. Therefore, we prescribe the following scalings for the dimensional variables:

$$\begin{aligned} x &= \hat{x}S \\ y &= \hat{y}S \\ z &= \hat{z}\delta = \hat{z}S/A_F \\ t &= \hat{t}/\Omega_o \\ (u,v,w) &= (\hat{u},\hat{v},\hat{w})u_o \\ \rho &= \rho_c\hat{\rho} \end{aligned} \tag{3}$$

where carets denote dimensionless variables and $A_F = S/\delta$ is the density field aspect ratio.

Sediment transport by the fluid velocity field, (u, v, w), can then be expressed by the nondimensional Fickian-based advection-diffusion equation as follows:

$$\begin{aligned} \frac{\Omega_o\delta^2}{\epsilon}\frac{\partial\hat{\rho}}{\partial\hat{t}} = \frac{\partial^2\hat{\rho}}{\partial\hat{z}^2} - R_F\left[\left(\hat{w} + \frac{\omega_o}{u_o}\right)\frac{\partial\hat{\rho}}{\partial\hat{z}} + \hat{\rho}\frac{\partial\hat{w}}{\partial\hat{z}}\right] \\ - \frac{R_F}{A_F}\left(\hat{\rho}\frac{\partial\hat{u}}{\partial\hat{x}} + \hat{u}\frac{\partial\hat{\rho}}{\partial\hat{x}} + \hat{\rho}\frac{\partial\hat{v}}{\partial\hat{y}} + \hat{v}\frac{\partial\hat{\rho}}{\partial\hat{y}}\right) \\ + \frac{1}{A_F^2}\left(\frac{\partial^2\hat{\rho}}{\partial\hat{x}^2} + \frac{\partial^2\hat{\rho}}{\partial\hat{y}^2}\right) \end{aligned} \tag{4}$$

where $R_F = u_o\delta/\epsilon$ is the mass flux Reynolds number equal to a ratio of advective to diffusive mass fluxes and ϵ is the mass diffusivity. Under the prototype conditions typical of the lower depths of estuaries along the U.S. west coast as encountered in Section 7, we take:

$$\begin{aligned} u_o &= O(10 \text{ cm/sec}) \\ \omega_o &= O(10^{-2} \text{ cm/sec}) \\ \Omega &= O(10^{-4} \text{ sec}^{-1}) \\ h &= O(10^2 \text{ cm} - 10^3 \text{ cm}) \\ \delta &= O(10 \text{ cm}), \\ \epsilon &= O(1 \text{ cm}^2/\text{sec}) \\ c &>> O(\delta) \end{aligned} \tag{5}$$

The final order of magnitude argument in (5) sets a minimum size restriction on the wing. This is necessary to avert Hele-Shaw flow, (WERLE, 1973 and McMASTERS, 1974) and to assure that the wing circulation is large compared to that of the ambient near-bottom flow.

OUTER SOLUTION

In the outer domain, $\hat{x} \geq O(1)$, the lowest order solution follows from (4) when the channel flow is subjected to an $O(1/A_w)$ perturbation from a wing at a small angle of attack β. The perturbation from a wing in ground effect at a distance z = b above a plane surface was first represented by an image pair of lifting lines by

BETZ (1912). The velocity potential of this familar vortex system is written in terms of outer variables (3) as:

$$\phi = \hat{x} + \beta\left(\frac{\hat{z}}{A_F} - \frac{b}{S}\right) + \frac{\beta f(x)}{2A_w}\int_{-1}^{1} \frac{\left(\frac{\hat{z}}{A_F} - \frac{b}{S}\right)T(\zeta)}{\left(\frac{\hat{z}}{A_F} - \frac{b}{S}\right)^2 + (\hat{y} - \zeta)^2} \cdot \left\{1 + \frac{\hat{x}}{\sqrt{\hat{x}^2 + \left(\frac{\hat{z}}{A_F} - \frac{b}{S}\right)^2 + (\hat{y} - \zeta)^2}}\right\} d\zeta - \beta\left(\frac{\hat{z}}{A_F} + \frac{b}{S}\right) - \frac{\beta f(x)}{2A_w}\int_{-1}^{1} \frac{\left(\frac{\hat{z}}{A_f} + \frac{b}{S}\right)T(\zeta)}{\left(\frac{\hat{z}}{A_f} + \frac{b}{S}\right)^2 + (\hat{y} - \zeta)^2} \cdot \left\{1 + \frac{\hat{x}}{\sqrt{\hat{x}^2 + \left(\frac{\hat{z}}{A_f} + \frac{b}{S}\right)^2 + (\hat{y} - \zeta)^2}}\right\} d\zeta \quad (6)$$

where $T(\zeta)$ is a unit function defining the spanwise distribution of circulation; $f(x)$ is a unit function defining the rate of downstream decay of circulation in the trailing vortices and ζ is a dummy variable. Terms containing $(z+b)$ correspond to the image vortex system at $z = -b$. We have adopted herein the convention that the lift force due to the real vortex acts upward in the positive z direction for $\beta > 0$.

Equations (5) and (6) require a large, high aspect ratio wing, whence $A_F \gg A_w \gg 1$. Consequently, the advection-diffusion equation (4) may be written at lowest order:

$$\frac{\partial \hat{\rho}^{(0)}}{\partial \hat{z}^2} - \frac{R_F}{A_W}\left(\hat{w}^{(1)}\frac{\partial \hat{\rho}^{(0)}}{\partial \hat{z}} + \hat{\rho}^{(0)}\frac{\partial \hat{w}^{(1)}}{\partial \hat{z}}\right) = 0 \quad (7)$$

where $\hat{w}^{(1)} = A_F \partial\phi/\partial\hat{z}$ is the $O(1/A_w)$ induced velocity. Equation (7) is subject to boundary conditions which require:

$$\hat{\rho}^{(0)} = 1 \text{ at } \hat{z} = 0 \quad (8)$$

$$\hat{\rho}^{(0)} = \rho_t/\rho_c \text{ at } \hat{z} = h/\delta \quad (9)$$

With (6) a solution to equation (7) can be obtained by successive integrations, evaluating the integration constants according to the boundary conditions (8) and (9) to yield the following result in dimensional form:

$$\rho = \rho_c \exp\left\{\frac{2}{\epsilon A_w}[I_1(x,y,z) - I_1(0) + \frac{z}{h}I_1(0) - \frac{z}{h}I_1(h)] + \frac{z}{h}\log\frac{\rho_t}{\rho_c}\right\} \quad (10)$$

where $I_1(0) = I_1(x,y,z = 0)$; $I_1(h) = I_1(x,y,z = h)$ and (see equation 11).

Here Γ_0 is the circulation of the bound vortex of the wing and Γ is the circulation of the trailing vortices such that,

$$\Gamma_0 = u_0 C_l c \quad (12)$$

$$\Gamma = \Gamma_0 f(x) \quad (13)$$

C_l in equation (12) is the lift coefficient which shall be positive for a wing above the bottom which generates lift upward in the positive z-direction. This case shall be referred to herein as a "downwashing" wing. When $C_l < 0$, the lift is directed downward toward the bottom and these shall be referred to as "upwashing" wings. The decay rate, $f(x)$, for the circulation of the trailing vortices in (13) is due to the ground effect calculations of PEACE and RILEY (1983) for the case of a stress free boundary at $z = 0$. Their results by numerical integration give:

$$f(x) = 1 - \int_0^\infty \left\{u^{(0)} + \left(\frac{xC_l\sigma}{u_0S^2}\right)^{1/2} u^{(1)} + \left(\frac{xC_l\sigma}{u_0S^2}\right)\left(u^{(2)} + \frac{\partial^2 u^{(0)}}{\partial x^2}\right)\right\} dx = 1 + (5.410 \times 10^{-3})\left(\frac{xC_l}{A_wS}\right) - (6.670 \times 10^{-4})\left(\frac{xC_l}{A_wS}\right)^2 + (1.173 \times 10^{-5})\left(\frac{xC_l}{A_wS}\right)^3 - (9.241 \times 10^{-8})\left(\frac{xC_l}{A_wS}\right)^4 + (2.729 \times 10^{-10})\left(\frac{xC_l}{A_wS}\right)^5 \quad (14)$$

where σ is the diffusivity of momentum.

INNER SOLUTION

The outer solution (10) develops singular behavior as $\hat{x} \to 0$ due to the line singularity of

$$I_2(x,y,z) = \frac{u_0\delta A_F}{A_w}\sin\beta\left\{\left[\frac{x^2}{c^2} - \frac{(z-b)^2}{c^2} - T^2\right]^2 + \left[\frac{2x(z-b)}{c^2}\right]^2\right\}^{1/4}\sin\left\{\tan^{-1}\left[\frac{2x(z-b)}{x^2-(z-b)^2-T^2}\right]\right\} \quad (22)$$

$$+ \frac{u_0\delta A_F}{A_w}\sin(-\beta)\left\{\left[\frac{x^2}{c^2} - \frac{(z+b)^2}{c^2} - T^2\right]^2 + \left[\frac{2x(z+b)}{c^2}\right]^2\right\}^{1/4}\sin\left\{\tan^{-1}\left[\frac{2x(z+b)}{x^2-(z+b)^2-T^2}\right]\right\}$$

$$- \frac{Tu_0\delta A_F}{A_w}\sin\beta\tan^{-1}\left[\left(\left\{\left[\frac{x^2}{c^2} - \frac{(z-b)^2}{c^2} - T^2\right]^2 + \left[\frac{2x(z-b)}{c^2}\right]^2\right\}^{1/4}\cdot \sin\left\{\frac{1}{2}\tan^{-1}\left[\frac{2x(z-b)}{x^2-(z-b)^2-T^2}\right]\right\} + \frac{(z-b)}{c}\right) \Big/ \left(\left\{\left[\frac{x^2}{c^2} - \frac{(z-b)^2}{c^2} - T^2\right]^2 + \left[\frac{2x(z-b)}{c^2}\right]^2\right\}^{1/4}\cos\left\{\frac{1}{2}\tan^{-1}\left[\frac{2x(z-b)}{x^2-(z-b)^2-T^2}\right]\right\} + \frac{x}{c}\right)\right]$$

$$- \frac{Tu_0\delta A_F}{A_w}\sin(-\beta)\tan^{-1}\left[\left(\left\{\left[\frac{x^2}{c^2} - \frac{(z+b)^2}{c^2} - T^2\right]^2 + \left[\frac{2x(z+b)}{c^2}\right]^2\right\}^{1/4}\cdot \sin\left\{\frac{1}{2}\tan^{-1}\left[\frac{2x(z+b)}{x^2-z+b)^2-T^2}\right]\right\} + \frac{(z+b)}{c}\right) \Big/ \left(\left\{\left[\frac{x^2}{c^2} - \frac{(z+b)^2}{c^2} - T^2\right]^2 + \left[\frac{2x(z+b)}{c^2}\right]^2\right\}^{1/4}\cos\left\{\frac{1}{2}\tan^{-1}\left[\frac{2x(z+b)}{x^2-(z+b)^2-T^2}\right]\right\} + \frac{x}{c}\right)\right]$$

Equation 22.

fer through the fluid mud layer. The velocity at the top of the fluid mud layer must match the fluid velocity along the stress free boundary at $z = 0$. However at the bottom of the fluid mud layer, $z = -m$, the velocity must vanish, giving rise to shear stresses within the fluid mud. Because the fluid mud is in motion these shear stresses, τ, must already be in excess of the cohesive yield stress of the fluid mud. Under the assumption that the fluid mud behaves as a thin Bingham fluid, (VANONI, 1975, FAAS, 1985, WRIGHT and KRONE, 1987), this excess shear stress, $\tau - \tau_c$, will vary with the wing disturbance as:

$$\tau - \tau_c = \frac{\mu}{m}\left[\left(\frac{\partial\Phi}{\partial X}\right)^2 + \left(\frac{\partial\Phi}{\partial Y}\right)^2\right]^{1/2}_{z=0} \quad (24)$$

where μ is the apparent viscosity of the fluid mud.

There are a number of erosion theories which predict that the rate of erosion increases with increasing $\tau - \tau_c$. The exponential rate theories of PARTHENIADES (1965), CHRISTENSEN (1965), CHRISTENSEN and DAS (1973), RAUDKIVI and HUTCHISON (1974) and GULARTE (1978) were found to grossly underestimate the wing-induced erosion fluxes under the prototype conditions described in Section 7.0. This is consistent with the fact that these rate equations are based upon data from artificially placed beds which characteristically erode more slowly than naturally deposited beds, (MEHTA, *et al.*, 1982). The linear theories of KANDIAH (1974), ARULANANDAN (1975),

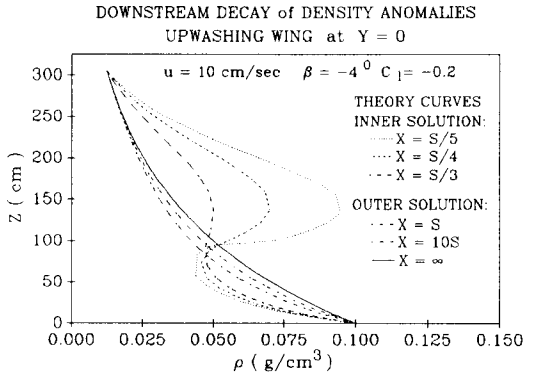

Figure 3 (A). Downstream decay of wing induced perturbations to the sediment component density as defined by equation (2). Calculations are based on: $\epsilon = 4.951$ cm^2/sec, $\rho_t = 0.0125$ g/cm^3 and $p_c = 0.10$ g/cm^3, and h = S = 304.8 cm.

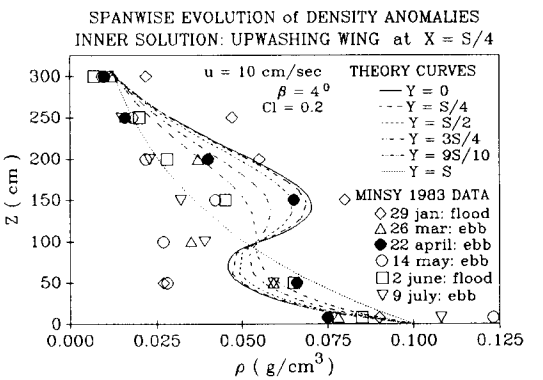

Figure 4 (A). Comparisons between theory and data for spanwise variations in the wing induced perturbations to the sediment component density in the near wake at X = S/4. Calculations are based on: $\epsilon = 4.951$ cm^2/sec, $\rho_t = 0.0125$ g/cm^3 and $\rho_c = 0.10$ g/cm^3, and h = S = 304.8 cm.

THORN and PARSONS (1980) and MEHTA (1981) can be calibrated from erosion rates observed over deposited beds because they are parameterized by a single empirically derived factor, α, according to:

$$E = \alpha\left(\frac{\tau - \tau_c}{\tau_c}\right) \qquad (25)$$

Here $\alpha > 0$ and positive values of erosion flux, E, correspond to erosion.

A contour map of the wing induced erosion flux from (24) and (25) for $C_l = +0.2$ is calculated in Figure 5a for prototype conditions typical of the experiment described in Section 7.0. Horseshoe-like erosion features are predicted in the near wake, due to the action of the horizontal induced velocity components. Such erosion is independent of the sign of the lift coefficient. However, erosion alone fails to account for shoaling details which might occur further downstream in response to an increased level of suspended sediment from mobilized bed material.

The deposition rate at z = m is directly proportional to the abundance of suspended sedi-

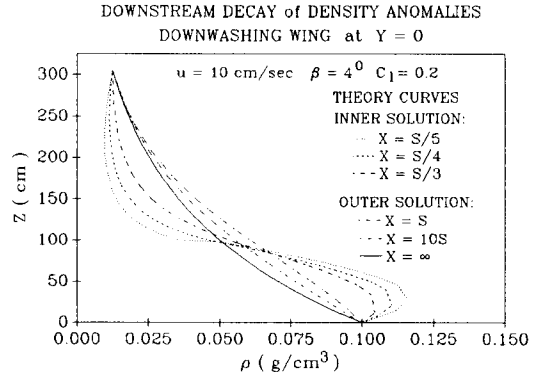

Figure 3 (B). Downstream decay of wing induced perturbations to the sediment component density as defined by equation (2). Calculations are based on: $\epsilon = 4.951$ cm^2/sec, $\rho_t = 0.0125$ g/cm^3 and $p_c = 0.10$ g/cm^3, and h = S = 304.8 cm.

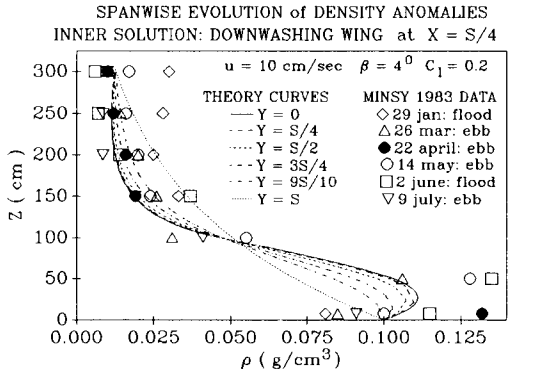

Figure 4 (B). Comparisons between theory and data for spanwise variations in the wing induced perturbations to the sediment component density in the near wake at X = S/4. Calculations are based on: $\epsilon = 4.951$ cm^2/sec, $\rho_t = 0.0125$ g/cm^3 and $\rho_c = 0.10$ g/cm^3, and h = S = 304.8 cm.

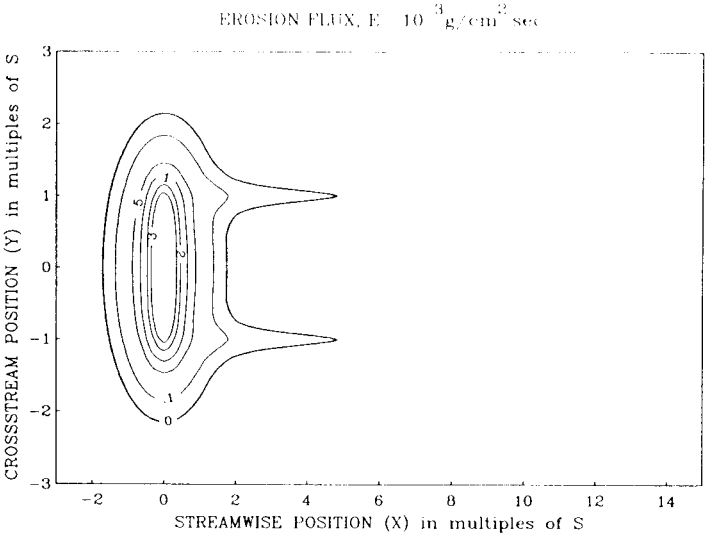

Figure 5. Contour maps of the erosion and deposition fluxes induced by a wing with $A_w = 5$ and $C_l = +0.2$ at a mooring elevation of b = 100 cm in a 10 cm/sec mean flow (A) Erosion flux for $\mu = 3.06 \times 10^{-2}$ gm/cm sec; $\tau_c = 0.5$ dynes/cm^2 and $\alpha = 2.356 \times 10^{-4}$ g/cm^2 sec.

ment near the bottom, (ARIATHURAI and KRONE, 1976, and COLE and MILES, 1983). This abundance is determined by the mass fluxes across the lutocline at z = 0. The flux of suspended sediment entering the fluid mud layer due to settling under gravity is $-\rho\omega_0$. These downward directed settling fluxes are the only mass fluxes considered by EINSTEIN and KRONE (1962), or MEHTA (1989) when accounting for deposition in the low turbulence environment of a settling column or laboratory flume. However in the high turbulence environment of a vortical wake in a natural estuary, vertical transport due to eddy diffusion must surely become important, especially along the strong density gradients in the neighborhood of the lutocline. The net of settling and diffusive fluxes across the lutocline determines the rate of change of suspended sediment in the fluid mud layer. However, there is only a finite probability, p(0,1), that this suspended sediment will actually stick to the bed at z = −m and consolidate to some ultimate saturation density ρ_s, (KRONE, 1962). Therefore the deposition flux, D, (including vertical diffusion and consolidation), may be written:

$$D = \frac{-K_s\rho_c g + p(0,1)\left\{\rho_c\omega_0 - \epsilon\frac{\partial\rho}{\partial z}\Big|_{z=0}\right\}}{(1 - \rho_c/\rho_s)} \quad (26)$$

Here positive values for D correspond to deposition while negative values indicate entrainment.

With equations (10) and (21) in (26), wing induced deposition fluxes in the inner, D_i, and outer domains, D_o, become:

$$\begin{pmatrix} D_o \\ D_i \end{pmatrix} = \frac{-K_s\rho_c g + p(0,1)}{(1 - \rho_c/\rho_s)}\left[\rho_c\omega_0 - \frac{\rho_c}{S}\left\{\frac{2}{A_w}\begin{pmatrix} I_1(S) - I_1(0) \\ I_2(S) - I_2(0) \end{pmatrix} - \epsilon\log\frac{\rho_t}{\rho_c}\right\}\right] \quad (27)$$

A contour map of the deposition flux induced by a downwashing wing at $C_l = +0.2$ is given in Figure 5b for the prototype conditions described in Section 7.0. We find that the deposition is enhanced in the wake trail when C_l is positive. In this case, the downwash behind the wing has reduced or even reversed the density gradient at the lutocline, (see Figure 3b), so that upward diffusion from the fluid mud layer is either greatly diminished or turned around to augment settling. However, when C_l becomes negative (upwashing), downstream entrain-

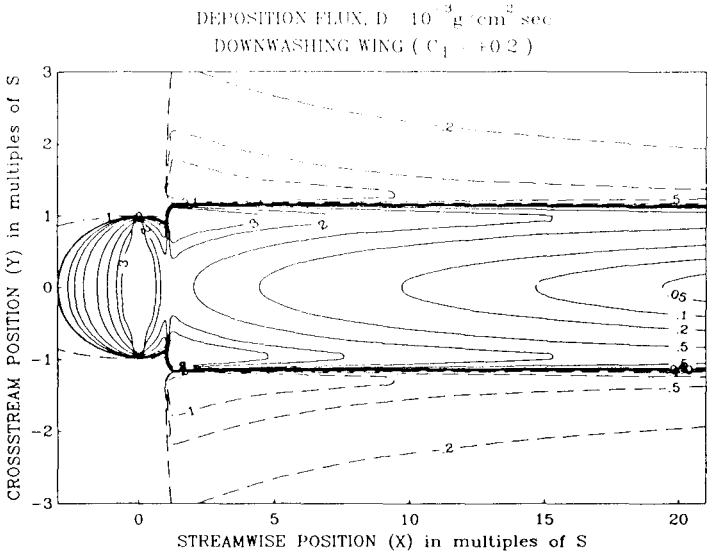

Figure 5 (B). Deposition flux for ϵ = 4.951 cm^2/sec. ω_o = 0.035 cm/sec, ρ_t = 0.0125 g/cm^3, ρ_c = 0.10 g/cm^3, and ρ_s = 1.2 g/cm^3, h = S = 304.8, and p(0,1) = 1.

ment occurs in both the inner and outer domain as a consequence of enhanced upward diffusive fluxes along density gradients which have been rendered more negative by the presence of the wing, see Figure 3a.

Over sufficiently long periods of time (many tidal cycles), the average shoaling flux, J, is the net resultant of the mean erosion and deposition fluxes, or

$$\bar{J} = \bar{E} - \bar{D} \qquad (28)$$

where overbars denote time averages. Here negative values of $\bar{J}$ correspond to shoaling or losses in the mean depth of water while positive values denote scour or depth gains. Comparisons of the shoaling performances between upwashing and downwashing wings at equal and opposite C_l are shown in plots of shoaling flux from (28) along the axis of the wake trail in Figure 6 and across the wake at x = S/3 in Figure 7. We find that the upwashing wing (C_l < 0) is predicted to be the most efficient configuration for scour or depth maintenance. The upwashing wing maintains positive shoaling fluxes all along the wake trail as a result of erosion in the near wake and entrainment in the far wake. This action extends beyond the wing tips in consequence of roll-up of the tip vortices.

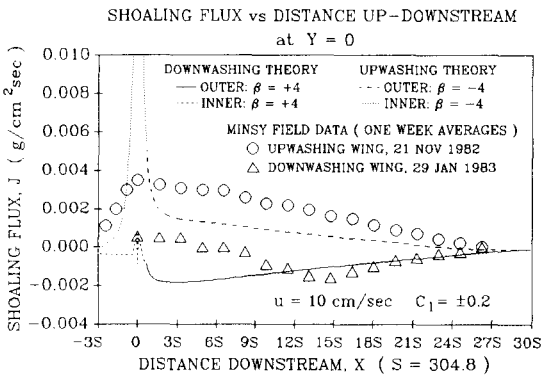

Figure 6. Comparison of shoaling flux theories and measurements along the axis of the wake trail for both downwashing (β = +4^0) and upwashing wings (β = − 4^0). Theory curves based on same parameterizations as in Figure 5.

The downwashing wing, on the other hand, appears to be so effective in advecting suspended sediments toward the bottom that deposition overwhelms erosion along much of the wake trail.

The induced velocity field of the wing disturbs future bottom profiles by fundamentally different mechanisms when causing erosion vs pre-

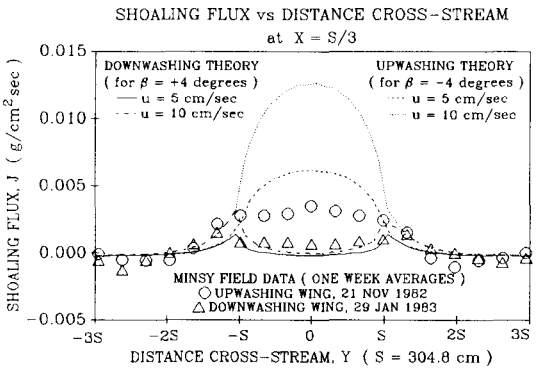

Figure 7. Comparison of shoaling flux theories and measurements across the wake trail at X = S/3. Theory curves based on a spanwise circulation distribution for a tapered wing according to (23) and parameterizations as in Figure 5.

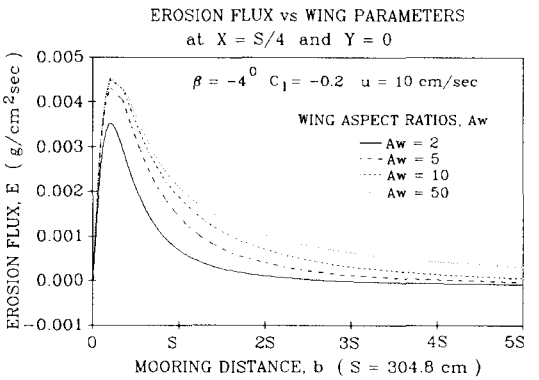

Figure 8. Variations of erosion and deposition fluxes with wing aspect ratio and mooring elevation. (A). Erosion flux at X = S/4.

venting deposition. In the case of erosion, the tangential velocities of the wing vortex system disturb the bottom directly by elevating the shear stresses in the fluid mud layer above the cohesive yield stress of the immobile bed. To prevent deposition the normal components of the induced velocities indirectly disturb future bottom profiles through their action on the density gradients above the lutocline. These normal induced velocities cannot directly cause advective fluxes of sediment across the lutocline because of vanishing normal flow along the stress free boundary at z = 0. By either mechanism shoaling is minimized by any given flow u_o by maximizing the C_l which the wing can generate in ground effect. Thus the sensitivity of the wing's lift-drag polar to both boundary proximity and low Reynolds numbers is critical, with little existing airfoil research as such to support optimal design selections.

The question of an optimal mooring elevation and wing aspect ratio is dependent upon the relative importance of erosion vs deposition in determining future bottom profiles. Erosion, which prevails near the wing, is maximized by mooring elevations relatively close to the lutocline, b = 0.25S, and increases slightly with increasing wing aspect ratio as shown in Figure 8a. Very little improvement in maximum E occurs for $A_w > 5$. This behavior is dominated by the vortex sheet of the wing. Lower mooring elevations increase the near wake tangential velocities over the bed and hence the magnitude of the shear stress within the fluid mud layer. Higher wing aspect ratios diminish tip loss effects near Y = 0. On the other hand, deposition is minimized at mooring elevations somewhat further above the lutocline, at b = 0.8S, and decreases rapidly with decreasing wing aspect ratio, as in Figure 8b. Since the deposition flux will be found to account for shoaled bottom profiles in the far wake, see Experiment section, such dependence on b and A_w is explicable in terms of the vertical velocities induced by the trailing vortices. Small mooring elevations and large wing aspect ratios tend to diminish the vertical induced velocities, with corresponding increases in the minimum attainable deposition flux.

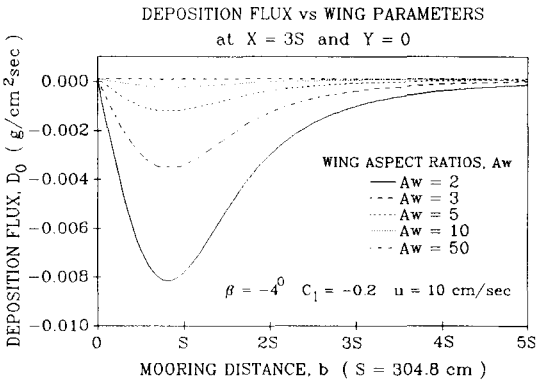

Figure 8 (B). Deposition flux at X = 3S. Parameterizations as in Figure 5, with h = 5S.

EXPERIMENT

Three buoyant wings were moored 100 cm above the initial bottom elevation of the Napa River at a mean depth of 10 meters. The configuration of the wings and their moorings is shown in Figure 1. Each wing was constructed of 1.6×10^{-1} gm/cm^3 urethane foam reinforced by steel tendons and ribs. The semi-span was made large relative to the floc layer thickness, S = 3.05 meters, so that large density field aspect ratios are compatible with (5). A large wing aspect ratio was required to remain within the purview of the theory and to maximize erosion. However, the need for an adequate wing cord to satisfy (5) and subsequent ordering arguments dictated a compromise selection for the wing aspect ratio of $A_w = 5$, making the mean semi-cord c = 0.61 meters.

Because low wing Reynolds numbers were anticipated in the slow moving, highly viscous floc layer, a stall resistant model airplane airfoil, the HQ-3.5/12, was employed (QUABACK, 1983). This airfoil also had the advantage of a nearly constant pitching moment coefficient over a wide range in angle of attack, allowing the use of a single point mooring as diagramed in Figure 1. The mooring point incorporated a swivel joint permitting complete rotational freedom to changes in current direction. The mooring point position and angle of attack were also fully adjustable by means of a pair of opposed turnbuckles under tension. The mooring attachment points were on the suction side of the upwashing wings with $\beta = -4°$, corresponding to $C_l = -0.2$ acting downward against the buoyancy. The downwashing wings were moored from the pressure side with $\beta = +4°$, so that $C_l = +0.2$ acting against the mooring tension. To maintain pitch, roll and yaw stability about this single point mooring, the wing plan form was configured with 30° of sweep back, 5° of dihedral, and small vertical stabilizers on each wing tip.

Two upwashing wings and one downwashing wing were installed in an 80 x 56 meter test area on November 11, 1982. The test area and a pair of 75 x 50 memter control areas were monitored by fathometer soundings, water sampling and diver inspection until November 6, 1983. The initial bottom topography in the test area was as shown in Figure 9a prior to wing installation. These contours were derived from grid surveys using a 40 kHz fathometer. The test area was abreast of Dry Dock #1 at the Mare Island Naval Shipyard (MINSY) and was bordered by a sheet pile quay wall along the shoreward side. The two upwashing wings were moored at points A and B in Figures 9a and 9b while the downwashing wing was moored at point C.

Two Marsh-McBirney electromagnetic current meters were placed at the mooring elevation, b = 100 cm, above the bottom at the ebb and flood ends of the test area. Seven months of current records indicated that the near bottom currents were modulated by tidal action, consistent with assumptions of time variability made in (5). Peak current amplitudes were O(20 cm/sec) while mean currents were $u_o \simeq 10$ cm/sec.

To measure the in situ values of (ρ_t, ρ_c, ρ_s), bottom cores and water samples of the lower portion of the water column were collected throughout the experiment according to a schedule regulated by barge and ship movements along the river. Each sample volume, O(500 ml), was determined to O(0.5 ml) accuracy and subsequently suction filtered through #1 Whatman filter paper with an 11 micron pore size. After ashing and drying in an oven for 24 hours to remove organics and absorbed water, the mass of sediment retained by the filter paper was determined with a Mettler analytical balance to $O(10^{-5}$ g) accuracy. The ratio of sediment mass to total sample volume gave the sediment component densities equivalent to equation (2).

The test period coincided with the 1983 El Nino when regional rainfall and sediment abundance in the Napa River were at 100 year record levels, (USGS, 1983). During the high siltation period between November 1982 and July 1983, the shoaling rates in two distinctly different control areas were monitored. One of these control areas (Pier 21) was located in a quiet water cul-de-sac where there were no measurable bottom currents and hence no erosion. Here the mean shoaling flux was found to be:

$$\bar{J} = -\bar{D} = \rho_s \frac{\partial \bar{\eta}}{\partial t} = -1.185 \times 10^{-4} \text{ gm/cm}^2 \text{ sec} \quad (29)$$

where η was the vertical position of the bed from 40 kHz fathometer soundings. From this

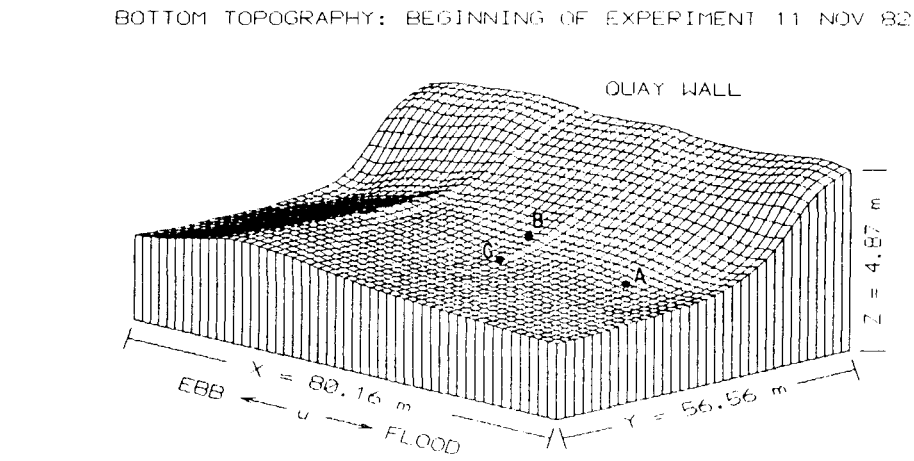

Figure 9 (A). Comparison of initial and final bottom configurations during the prototype wing test. Upwashing wings ($C_l < 0$) were moored at points A & B. A downwashing wing ($C_l > 0$) was moored at point C.

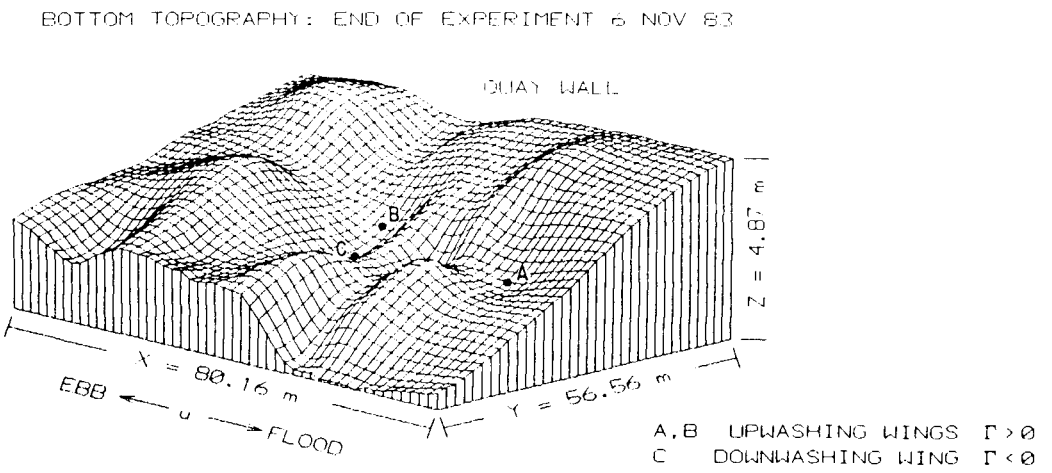

Figure 9 (B). Comparison of initial and final bottom configurations during the prototype wing test. Upwashing wings ($C_l < 0$) were moored at points A & B. A downwashing wing ($C_l > 0$) was moored at point C.

observed shoaling flux the mass diffusivity was calibrated by solving equation (27) for the case of no-wings, $I_1 = I_2 = 0$, to get:

$$\epsilon = \frac{\bar{J}(1 - \rho_c/\rho_s) - K_s\rho_c g + \rho_c\omega_0}{\frac{\rho_c}{S} \cdot \log\left(\frac{\rho_t}{\rho_c}\right)} = 4.951 \text{ cm}^2/\text{sec} \quad (30)$$

Here, $\rho_t = 0.0125$ g/cm^3, $\rho_c = 0.100$ g/cm^3, and $\rho_s = 1.2$ g/cm^3 derived from averages of the in situ water samples collected in the control areas throughout the duration of the experiment. The sedimentation coefficient was taken as $K_s = 4 \times 10^{-13}$ sec after the work of FUJITA (1962). A characteristic settling velocity in equation (30) of $\omega_0 = 0.035$ cm/sec was based upon a 25 micron median aggregate size determined by scanning electron microscopy size analysis of the suspended load in the Napa River water samples.

The fluid mud parameters (μ,m,τ_c) were derived from grab samples recovered by divers. These samples were placed immediately in a Brookfield Viscometer, giving average values of $\mu = 3.06 \times 10^{-2}$ gm/cm sec and $\tau_c = 0.5$ dynes/cm^2. The thickness of the fluid mud layer was estimated to be O(15 cm), based upon the band of abrasion appearing on the upper portions of the vertical steel members of the shear plate as shown in Figure 1. With these values and the calibrated mass diffusivity (30), we have invoked (27) and (28) to back out the erosion flux contribution to the observed mean shoaling flux at the remaining control area (Berth 7), and found that $\alpha = 2.356$ gm/cm^2 sec.

Sediment component densities measured approximately x = S/4 downstream of the upwashing wing-B are compared with the inner solution calculations (21) in Figure 4a. The majority of these measurements are found to lie in the envelope of the theory curves. This envelope is believed to be the correct standard for comparison because precise cross stream positioning during water sample collection was difficult while surface currents were running. In general the data show high levels of suspended sediments raised above the upwashing wing and locally smaller levels at the mooring elevations, b = 100 cm. Such a near bed density distribution is not typical of Nature. Thus an inversion layer has been created in the region above the floc layer by the upward advection of the near wake in reaction to downward lift.

Comparisons between theory and measured sediment component densities observed at x = S/4 downstream from downwashing wing-C are shown in Figure 4b. Samples yielding this data were gathered on the same days as those in Figure 4a and show comparable values above and at the bottom of the floc layer. However, in Figure 4b a high density toe of suspended sediment is found below the wing and above the presumed lutocline at z = 0. Some of the sediment component densities in this toe are actually in excess of those found at the lutocline. This, too, is an unnatural finding. Acoustic evidence of this near-bottom high density suspension is found downstream (LHS) of the echo return for wing-C in Figure 10a. The 40 kHz acoustic waves are known to back scatter from strong density gradients like those appearing above the bottom in Figure 4b, (KIRBY and PARKER, 1974). Hence, the downstream acoustic image in Figure 10a is qualitatively consistent with the measured density anomalies near the bed in Figure 4b. Together, these observations support theoretical expectations that downwashing wings tend to drive suspended sediment down into the lower portions of the floc layer, causing an inversion layer below the wing.

Shoaling flux estimates derived from 40 kHz fathograms are compared with theory in Figures 6 and 7. One of these fathograms is shown in Figure 10b, taken along the centerline of the wake, (y = 0), behind an upwashing wing, B. The upwashing wings ($C_l < 0$) were found to diminish downstream shoaling while the downwashing wings ($C_l > 0$) were found to cause downstream accretion, although the outer solution for the shoaling flux tends to underestimate both. The momentum diffusivity was fixed at $\sigma = 3\epsilon$ in order to match the length of the scour trail with the data. The data were based upon one week averages shortly after the wing installations were completed, when the erosion fluxes were relatively large.

In the near wake of the wing, the inner solution of the shoaling flux was found in Figures 6 and 7 to overestimate the observed erosion due to an upwashing wing by a considerable amount. This is believed to be due to the assumption of a constant τ_c when posing the erosion flux according to (25). As erosion cuts into the bed, denser more consolidated mud is exposed which has a higher cohesive yield stress and is thus more resistant to erosion than predicted by the calculations in Figures 6 and 7. This argument is supported by the fact that the smaller positive shoaling fluxes which do not entail erosion cuts as deeply into the bed are predicted reasonably well in the near wake of a downwashing wing. Unfortunately, the calculation does not account for the unshoaled intermediate region between $2S < x < 8S$ behind a downwashing wing. This may again be due to cross stream positioning errors if the fathometer sweep was performed along one of the erosive tails of the horseshoe at Y = S in Figure 5a rather than along the centerline of the wake, Y = 0.

The rate of erosion of naturally deposited beds typically decreases with increasing time and may eventually arrest altogether, (MEHTA *et al.*, 1982). Not only does erosion expose denser, more erosion-resistent material, it also increases the effective mooring elevation,

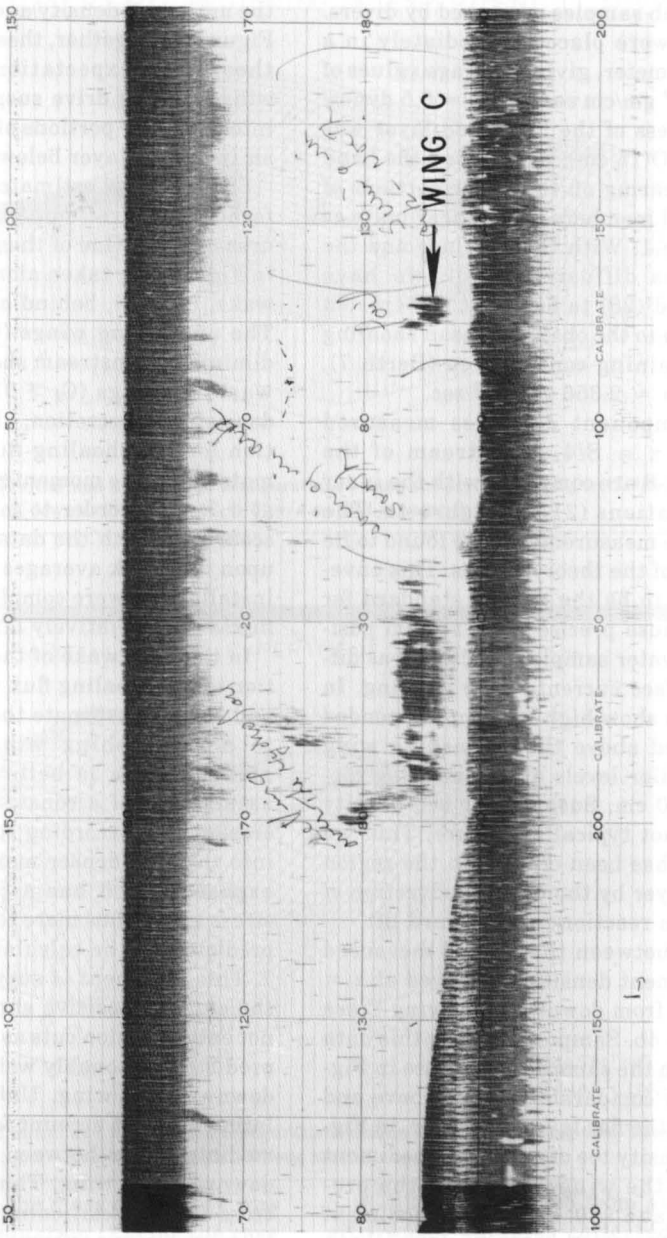

Figure 10. 40 kHz fathograms of the moored wings. (A). Shows accoustic reflection from a dense suspension of sediment behind downwashing wing C at a $C_l = +0.2$.

thereby reducing further erosion while increasing downstream deposition in accordance with the results of Figures 8a and 8b. The image method calculations also become increasingly inaccurate as the bottom deviates from a plane configuration. Flow divergence over wing induced scour holes will surely reduce the circulation which the wing can generate. These factors all work together over time to slow or arrest erosion. A final steady state bottom con-

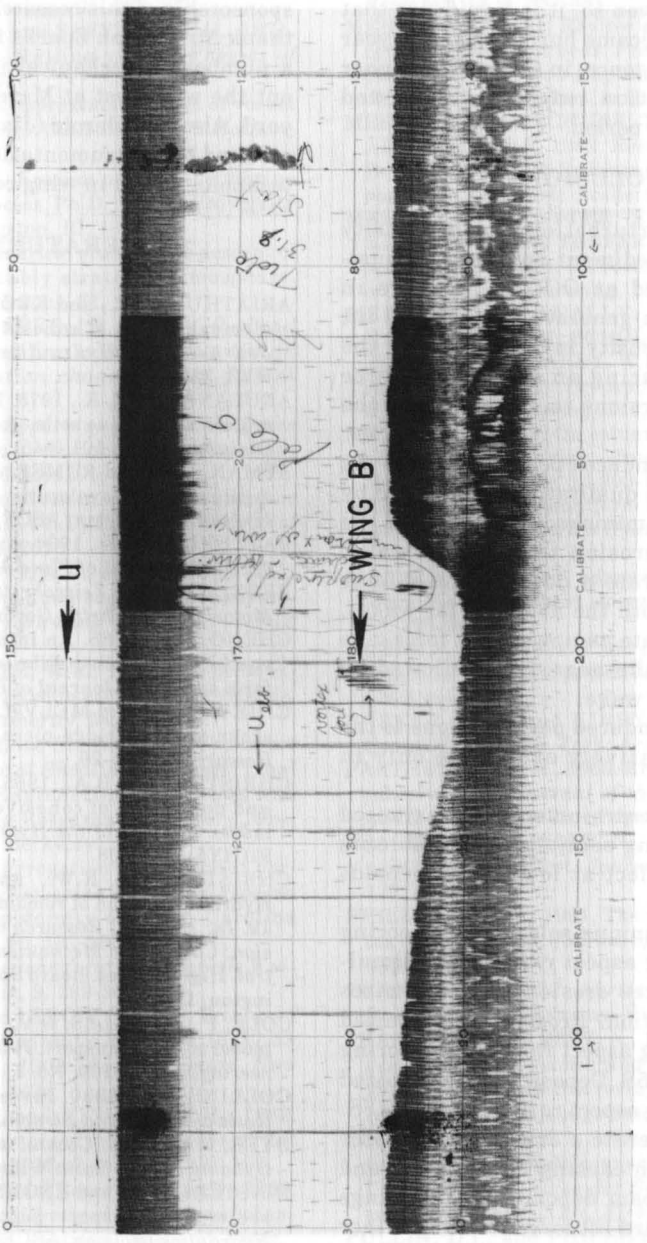

Figure 10. (B). Shows the scour trail plotted in Figure 6 induced by upwashing wing B.

figuration as shown in Figure 9b was found 12 months later. The long-term erosion process has produced local scour holes in the neighborhood of both downwashing and upwashing wings alike. Such features are qualitatively similar to the erosion simulation depicted in Figure 5a. None of the long extended scour trails associated with entrainment and diminished deposition behind an upwashing wing are still in evidence in the final steady state bottom configuration. Thus deviations from a flat bottom in consequence of near-wake erosion

appears to greatly inhibit vertical mass transport in the wake. Even so, it is significant that none of the wings became buried after one year of continual submergence, in spite of the higher than normal siltation rates that persisted throughout the test period.

CONCLUSIONS

Wing induced perturbations to the density field of suspended sediment appear to be qualitatively accounted at $O(R_F/A_w)$. Wings in ground effect which generate a downward lift force give rise to density inversions above the wing. Wings producing an upward lift force cause density inversions to appear below the wing.

Short term wing induced perturbations to the bottom appear to be qualitatively explained by entrainment and diminished deposition in the far wake and by erosion in the near wake. Wings which generate a downward lift force induce erosion in both the near and far wakes. Wings which generate an upward lift force give rise to erosion in the near wake followed by accretion in the far wake.

Long term wing induced perturbations to the bottom are qualitatively explicable only in terms of erosion.

Both erosion and entrainment are maximized by maximizing wing section lift coefficients while in ground effect at low wing Reynolds numbers.

There exists no unique selection of mooring elevation and wing aspect ratio which simultaneously maximizes erosion and minimizes downstream deposition. Erosion is maximized by maximizing wing aspect ratio for a mooring elevation of b = 0.25S. Deposition is minimized by minimizing wing aspect ratio with b = 0.8S.

Wings which generate a downward lift force are more effective in causing local erosion and retarding downstream deposition than wings generating an upward lift force. Because either effect is limited to a wake trail whose cross-stream dimension is of the order of a wing span, large areas of channel bottom will require mass arrays of wings with overlapping wakes (like a flock of birds), in order to control shoaling.

ACKNOWLEDGEMENTS

The authors are indebted to Dr. Eugene Silva and Dr. Steven Ramberg of the Office of Naval Research, Code 1121, for technical support and sponsorship of this research. We further wish to thank Mr. Joseph Sparks for diver support and a number of mechanical innovations throughout the wing test at Mare Island Naval Shipyard. Also, Dr. Darold (Jim) Palmer is specially credited for instrumentation and concrete mold technology used in wing construction.

LITERATURE CITED

ARIATHURAI, R., and KRONE, R.B., 1976. Finite element model of cohesive sediment transport, *Journal of the Hydraulics Division*, ASCE, 102, HY3, 323-338.

ARULANANDAN, K., 1975. Fundamental aspects of erosion of cohesive soils. *Journal of the Hydraulics Division*, ASCE, 101 (445), 635-639.

APMAN, R.P., and RUMER, R.R., 1970. Diffusion of sediment in developing flow. *Journal of the Hydraulics Division*, ASCE, 96, HY1, 109-123.

BATCHELOR, G.K., 1964. Axial flow in trailing line vortices. *Journal of Fluid Mechanics*, 20, 645-658.

BETZ, A., 1912. *Zeitschrift fur Flugtechnik und Motorluftschiffahrtm*, Germany, 13, 86p.

CHENG, K.J., 1985. An integrated suspended load equation for non-equilibrium transport of nonuniform sediment. *Journal of Hydrology*, 79, 359-364.

CHIEW, J.M., and MELVILLE, B.W., 1987. Local scour around bridge piers. *Journal of Hydraulic Research*, 25, 15-26.

CHRISTENSEN, B.A., 1965. Discussion of erosion and deposition of cohesive soils (by E. Parthenaides). *Journal of the Hydraulics Division*, ASCE, 91(HY5), 301-308.

CHRISTENSEN, R.W., and DAS, B.M., 1973. Hydraulic erosion of remolded cohesive soils, pp. 8-19. *In:* National Research Council, (ed.), *Soil Erosion: Causes and Mechanisms, Prevention and Control*. Highway Res. Board Special Report 135, Washington, D.C.

COLE, P., and MILES, G.V., 1983. Two-dimensional model of mud transport. *Journal of Hydraulic Engineering*, ASCE, 109, No. 1, 1-12.

COLLINS, T.J., 1980. Investigating bridge scour. *Railway Track and Structure*, 76p.

DYER, K.R., 1985. *Coastal and Estuarine Sediment Dynamics*, New York: Wiley, 342p.

EINSTEIN, H.A., and KRONE, R.B., 1961. Estuarine sediment transport patterns. *Journal of the Hydraulics Division*, ASCE, 87, HY2, 1451-1461.

EINSTEIN, H.A., and KRONE, R.B., 1962. Experiments to determine the models of cohesive sediment transport in salt water. *Journal of Geophysical Research*, 67, 4, 1451-1461.

FAAS, R.W., 1985. Time and density-dependent properties of fluid mud suspensions, NE Brazilian continental shelf. *Geo-Marine Letters*, 4, 147-152, 184-185.

FUJITA, H., 1962. *Mathematical Theory of Sedimentation Analysis*. York: Academic 315p.

GARRAD, P.N., and HEY, R.D., 1987. Boat traffic,

sediment resuspension and turbidity in a broadland river. *Journal of Hydrology*, 95, 289-297.
GOVINDARAJU, S.P., and SAFFMAN, P.G., 1971. Flow in a turbulent trailing vortex. *Physics of Fluids*, 14, 2074-2080.
GREEN, G.C., 1985. An approximate model of vortex decay in the atmosphere. *AIAA 12th Flight Mechanics Conference*, 85-1835.
GULARTE, R.C., 1978. Erosion of cohesive marine sediment as a rate process. Ph.D. Thesis, University of Rhode Island, Kingston, RI, 190p.
HILL, F.M., 1975. A numerical study of the descent of a vortex pair in a stably stratified atmosphere. *Journal of Fluid Mechanics*, 71, 1-13.
JENKINS, S.A., and SPARKS, J.B., 1985. *Method and apparatus for impeding fine sediment deposition in harboro and navigation channels*. U.S. Patent #4,560,304.
JENKINS, S.A., 1987. *Apparatus for impending fine sediment deposition in harbor and navigation channels*. U.S. Patent #4,661,013.
KANDIAH, A., 1974. Fundamental aspects of surface erosion of cohesive soils. Ph.D. Thesis, University of California, Davis, CA, 261p.
KERSSENS, M.J.; PIRNS, A.D., and van Rign, L.C., 1979. Model for suspended sediment transport. *Journal of the Hydraulics Division*, ASCE 105(HY5), 461-476.
KIRBY, R., and PARKER, W.R., 1974. Sea-bed density measurements related to echo-sounder records. *Dock and Harbour Authority*, 54, 423-424.
KRONE, R.B., 1962. *Flume Studies of the Transport of Sediment in Estuarial Shoaling Processes*. Final report, Hydraulics Engineering Laboratory and Sanitary Engineering Research Laboratory, University of California, Berkeley.
KRONE, R.B., 1978. Aggregation of suspended particles in estuaries. *In: Estuarine Transport, Process*, B. Kjerfve, (ed.). University of South Carolina Press, Columbia, SC, pp. 177-190.
LAGALLY, M., 1929. *Zeitshrift fur Angeuanetle Wulhewatch und Mechanik*, 9, 299-305.
LAMBERMONT, J., and LEBON, G., 1978. Erosion of fine soils. *Journal of Hydraulic Research*, 16, 27-33.
LANCHESTER, F.W., 1908. *Aerodynamics*, New York: Van Nostrand, 442p.
MacLENNAN, A.S.M., and VINCENT, J.H., 1982. Transport in the near aerodynamic wakes of flat plates. *Journal of Fluid Mechanics*, 20, 185-197.
MARINE BOARD, (National Research Council). 1983. *Criteria for the depths of dredged navigational channels*. Washington, D.C., National Academy Press.
MATTEI, A., and SANTORO, E., 1974. Numerical computations of wake vortices behind lifting surfaces. *International Conference of Aeronautical Science*, pp. 244-249.
McCORMICK, B.W., 1979. *Aerodynamics, Aeronautics, and Flight Mechanics*. New York: Wiley, 653p.
McMASTERS, J.H., 1974. An analytic survey of low-speed flying devices—natural and man-made. *Journal of Technical Soaring*, 111 (4), 17-39.
MEHTA, A.J., and PARTHENIADES, E., 1975. An investigation of the depositional properties of flocculated fine sediments. *Journal of Hydraulics Research*, 13, 4, 361-381.
MEHTA, A.J., 1981. Review of erosion function for cohesive sediment beds. *Proceedings First Indian Conference on Ocean Engineering*, Indian Institute of Technology, Madras, India, I, pp. 122-130.
MEHTA, A.J.;; PARCHURE, T.M.; DIXIT, J.G., and ARIATHURAI, R, 1982. Resuspension Potential of Deposited Cohesive Sediment Beds. *Estuarine Comparisons*. New York: Academic, 709p.
MEHTA, A.J., HAYTER, E.J.; PARKER, W.R.; KRONE, R.B., and TEETER, A.M., 1989. Cohesive sediment transport. I: Process description. *Journal of Hydraulic Engineering*, 115, (8), 1076-1093.
MEHTA, A.J.; McANALLY, W.H., JR.; HAYTER, E.J., TEETER, A.M.; SCHOLELLHAMER, D.; HELTZEL, S.B., and CAREY, W.P., 1989. Cohesive sediment transport. II: Application. *Journal of Hydraulic Engineering*, 115, (8), 1094-1112.
MEHTA, A.J., 1989. On estuarine cohesive sediment suspension behavior, *Journal of Geophysical Research*, 94, (C10), 14,303-14,314.
MEI, C.C., 1969. Nonuniform diffusion of suspended sediment. *Journal of the Hydraulics Division*, ASCE 95(HY1), 581-584.
MOORE, D.W., 1974. A numerical study of the roll-up of a finite vortex sheet. *Journal of Fluid Mechanics*, 63, 225-235.
NICHOLS, M.N., 1985. Fluid mud accumulation processes in an estuary. *Geo-Marine Letters*, 4, 171-176(1984-1985).
PARKER, W.R., and KIRBY, R., 1982. *Estuarine Comparisons*. New York: Academic, pp. 573-589.
PARTHENIADES, E., 1965. Erosion and deposition of cohesive soils. *Journal of the Hydraulics Division*. ASCE 91, (HY 1), Proc Paper 4204, pp. 105-139.
PEACE, A.J., and RILEY, N., 1983. A viscous vortex pair in ground effect. *Journal of Fluid Mechanics*, 129, 409-426.
PHILLIPS, W.R.C., 1981. The turbulent trailing vortex during roll-up. *Journal of Fluid Mechanics*, 105, 451-467.
PRANDTL, L., 1931. *Abriss der Stromungslehre*. Braunschweig, Germany: Vieweg, 223p.
PRANYTL, L., and BETZ, A., 1927. *Vier Abhandlungen zur Hydrodynamik und Aerodynamik*. Gottingen, Germany: Gelbstverlag des Kaiser Wilkelm Institute fur Stromungsforsching, 110p.
PRESNAK, W.J., 1977. Some special cases of potential flow around multi connected airfoils. *Bulletin de l'Academie Polenaise der Sciences*, Serie der Sciences Technique, XXV, 37-44.
PULLIN, D.I., and PHILLIPS, W.R.C., 1981. On a generalization of Kaden's problem. *Journal of Fluid Mechanics*, 104, 45-53.
QUABACK, H., 1983. *"HQ-Profile," Modell Technik Berater, MTB-7*. Verlag Fur Technik Und Handwerk GmDH., Baden-Baden, Germany, 70p.
RAUDKIVI, A.J., and HUTCHINSON, D.L., 1974. Erosion of kaolimite clay by flowing water. *Proceedings of the Royal Society of London*. A337, 537-554.
SAFFMAN, P.G., 1972. The motion of a vortex pair in a stratified field. *Studies in Applied Mathematics* LI, (2), 107-110.

SAFFMAN, P.G., 1973. Structure of turbulent line vortices. *Physics of Fluids*, 16, 1181-1188.
SQUIRE, H.B., 1965. The growth of a vortex in turbulent flow, *Aeronautical Quarterly*, 16, 302-306.
STAUFENBIEL, R., and KLEINERDAM, G., 1980. Longitudinal motion of low-flying vehicles in nonlinear flowfields. *International Conference of Aeronautical Science*, 293-308.
THORN, M.F.C., and PARSONS, J.G., 1980. Erosion of cohesive sediments in estuaries: an engineering guide. *Proceedings 3rd International Symposium Dredging Technology*, pp. 349-358.
USGS, 1983. *Water Resources Data for California*. U.S. Geological Survey, #CA-83-2.
VAN DYKE, M., 1964. Lifting-line theory as a singular-peturbation problem. *Journal of Applied Mathematics and Mechanics*, 28, 90-101.
VAN DYKE, M., 1975. *Perturbation Methods in Fluid Mechanics*. Stanford, California: Parabolic, 271p.
VANONI, V.A., (ed.), 1975. *Sedimentation Engineering*. New York: American Society of Civil Engineers, 745p.
WERLE, H., 1973. Hydrodynamic flow visualization. *Annual Review of Fluid Mechanics*, 5, 361-382.
WRIGHT, V.G., and KRONE, R.B., 1977. Laboratory study of mud flows. *Proceedings of National Conference on Hydraulic Engineering*, 237-242, (American Society of Civil Engineers, New York).
YALIN, M.S., 1977. *Mechanics of Sediment Transport*, Oxford: Pergamon, 290p.

□ RESUMEN □

Se muestra en este trabajo una teoría con correspondiente experimentación que describe la resuspensión de sedimentos finos debida a la acción de alerones anclados cerca del fondo de un estuario. Los cálculos mediante el método de las imagenes indican que el sistema de vórtices de un alerón puede ejercer dos efectos diferentes sobre la sedimentación del estuario: 1) Puede aumentar la tensión tangencial en las proximidades del alerón hasta una cantidad suficiente como para inducir la erosión de las capas de sedimento de fondo parcialmente consolidadas; y 2) puede promover transporte vertical que incremente o disminuya la sedimentación corriente abajo. Se ha encontrado que la sedimentación en la cola de la estela depende de la dirección de la fuerza de sustentación generada por el alerón. Los alerones que producen una fuerza de sustentación descendente limpian la región adyacente del fondo de sedimento suspendido y, por lo tanto, disminuye la sedimentación aguas abajo. Recíprocamente, los alerones que generan una fuerza de sustentación ascendente incrementan la concentración de sedimento suspendido cerca del fondo, incrementando por lo tanto la tasa de sedimentación aguas abajo. Se formulan las configuraciones de alerones óptimas que maximizan la erosión y minimizan la sedimentación. Las medidas de concentración detrás de prototipos de alerones son consistentes con las expectativas teóricas. Los cambios a corto plazo de la batimetría del fondo se ajustan en general con la erosión predicha en el dominio interior y con la menor acreción en el dominio exterior. *Department of Water Sciences, University of Cantabria, Santander, Spain.*

□ RÉSUMÉ □

Présente une expérimentation décrivant la resuspension des sédiments fins sous l'action d'ailes amarrées près du fond dans un estuaire. Les calculs réalisés par ajustement à des expansion d'images internes et externes indiquent que le vortex d'une aile peut exercer deux effets distincts sur la sédimentation estuarienne. 1) Il peut accroitre par une quantité suffisante la force de cisaillement du voisinage et induire une érosion des couches partiellement consolidées du fond. 2) Il peut promouvoir un transport vertical qui soit augmente, soit diminue le dépôt aval. Dans la traînée du sillage, le dépôt est dépendant de la force d'élévation entraînée par l'aile. Les ailes qui produisent une force d'élévation en aval provoquent le départ des sédiments fins en suspension près du fond et diminuent le dépôt aval. A l'inversé, les ailes engendrant une force vers le haut accroissent la densité des sédiments en suspension près du fond et accroissent donc le dépôt en aval. Les mesures de densité derrière les ailes du prototype coïncident avec ce qui pouvait être déduit de la théorie. Les changements à court terme des formes de fond coïncident généralement avec l'érosion prédite dans le domaine interne et avec une accrétion diminuée dans le domaine externe.—*Catherine Bressolier, Géomorphologie EPHE, Montrouge, France.*

□ ZUSAMMENFASSUNG □

Eine Theorie und ein begleitendes Experiment werden vorgestellt, die die Wiederaufnahme feinkörniger Sedimente als Suspensionsfracht aufgrund von Flügeln beschreiben, die am Grunde eines Ästuars verankert sind. Berechnungen zeigen, daß die Wirbelbildungen an einem solchen Flügel zwei verschiedene Auswirkungen auf die Sedimentation im Ästuar haben können: 1) Sie können die Schubspannungen in der Umgebung des Flügels um ein solches Ausmaß erhöhen, daß dadurch die Erosion von teilweise verfestigten Schichten am Ästuargrund ausgelöst wird; und 2) können sie den vertikalen Transport fördern, um eine stromabwärtige Ablagerung entweder zu steigern oder zu hemmen. Es ergab sich, daß die Sedimentation im Kielwasserbereich von der Richtung der Hubkraft abhängig ist, die von dem Flügel erzeugt wird. Flügel, die eine nach unten gerichtete Hubkraft bewirken, beseitigen Schwebgut in dem am Grunde angrenzenden Gebiet und vermindern dadurch die stromabwärtige Ablagerung. Umgekehrt vergrößern Flügel, die eine nach oben gerichtete Hubkraft bewirken, die Schwebgutdichte nahe dem Grunde und dadurch auch die stromabwärtige Ablagerungsrate. Bestmögliche Flügelgestaltungen werden vorgeschlagen, die die Erosion maximieren und die Ablagerung minimieren. Dichtemessungen bei Prototyp-Flügeln stimmen mit diesen theoretisch abgeleiteten Erwartungen überein. Kurzzeitige Veränderungen des Reliefs am Ästuarboden stehen im generellen Einklang mit der vorhergesagten Erosion im inneren und der verminderten Anlagerung im äußeren Flügelbereich.—*Helmut Brückner, Geographisches Institut, Universität Düsseldorf, F.R.G.*